International Journal of
Georesources and Environment
IJGE 2018 4(3): 147-152
http://ijge.camdemia.ca, ijge@camdemia.ca
Available at http://ojs.library.dal.ca/ijge
Research and Development and Industry

Pore Characteristics Analysis of Shale from Sichuan Basin, China

Ke Hu*, Helmut Mischo
Institute of Mining and Special Civil Engineering, TU Bergakademie Freiberg, Sachsen, Germany

Abstract: Pore characteristics are significant for shale gas exploration and production. In this paper, the method of field emission scanning electron Microscopes (FE-SEM) was applied to qualitatively describe minerals and pore structures of shale samples. Low pressure nitrogen adsorption-desorption and carbon dioxide adsorption were applied to analyse meso-pores and micro-pores respectively. Inter-particle pores are always associated with rigid mineral grains and intra-particle pores are mainly located in unstable minerals. The BET (Brunauer–Emmett–Teller) surface area of Longmaxi Formation (LMX) is 5.47m^2/gr and 16.33m^2/gr of Wufeng Formation (WF). N_2 and CO_2 adsorption shows that the diameter of micro-pores in the LMX and WF formation is approximately 1nm. Most meso-pores in WF formations range from 2nm - 20nm, while meso-pores existing in LMX formations range from 2nm - 30nm.

Keywords: gas shale, pore characteristics, Sichuan Basin

1 Introduction

Being characterised as a most promising unconventional type of gas and due to the evolution of horizontal drilling and hydraulic fracturing technology, shale gas has already attracted much attention, especially in the U.S. The production in the United States was 469.56 billion cubic meter (BCM) in 2016, representing 50% of the total gas production in the country (EIA). Meanwhile, Canada, China, Poland, Brazil among others have also started exploring for and producing shale gas. To reduce the extent of import reliance on energy, the Chinese government has carried out some exploration and production programs as well, in Sichuan Basin (Zou et al 2010).

Sichuan Basin that is located in the southeast side of China, has already started producing shale gas since 2009 as a pioneer. The Upper-Ordovician Wufeng Formations and Lower Silurian Longmaxi Formations marine shale consist the main shale gas reservoirs.

Compared to conventional gas reservoirs, shale gas can be found in reservoirs in three states: free and compressed gas in pores and fractures, adsorbed gas on the surface of organic matter and minerals, dissolved gas in water and organic matter (Ross and Bustin 2009).

Other than in conventional hydrocarbon reservoirs, shale gas can also be found as adsorbed gas (20-80%) (Ambrose et al 2012). Pores and micro fractures are the main adsorptive sites for adsorbed gas and channels for gas flow. Therefore, geometrical morphology and pore size distribution (PSD) are key factors for gas in place (GIP) prediction and production. In addition, pore characteristics are also significant for gas migration and application of depleted wells, such as in carbon dioxide sequestration. A better understanding of pore characteristics of the shale in Sichuan basin can provide more effective information for shale gas occurrence, stored capacity and transportation mechanisms.

Compared to conventional reservoir, sedimentary environments and the diagenetic process of gas shale are much more complicated. Accordingly, this leads to a more complicated pore structure and pore geometry. In recent years, researchers applied various kinds of methods to characterise the pore system of shale, including image analysis, intrusive and non-intrusive methods. Image analysis methods are widely applied for qualitative and quantitative analysis of pore geometry, based on techniques such as; field emission scanning electron microscopy (FE-SEM) (Houben et al 2016), focus iron beam scanning electron microscopy (FIB-SEM) (Bernard et al 2013, Kelly et al 2016), transmission electron microscopy (TEM) (Bernard et al 2013), atomic force microscopy (AMF) (Javadpour et al 2012) and focused ion beam-Helium ion microscopy (FIB-HIM) (Wu et al 2017). Such methods can provide directly visual images with high resolution to observe the nano-pores. Combined with serial slices and reconstruction software, these images can represent porosity and connectivity.

Intrusive methods include mercury injection (MIP), low pressure nitrogen adsorption, low pressure argon adsorption and low pressure CO_2 adsorption. Different methods have different detectable ranges, though limited by molecular. Generally, MIP and low pressure gas adsorption are combined to determine the wide range of pore size distribution. The International Union of Pure and Applied Chemistry (IUPAC 1994) classified pores as micro-pores

* Corresponding Author: Ke Hu, Email: huke1@mailserver.tu-freiberg.de, phone: +49 3731/393033

DOI: 10.15273/ijge.2018.03.024

(smaller than 2nm), meso-pores (2-50nm) and macro-pores (larger than 50nm) in diameter, respectively.

Non-intrusive methods involve nuclear magnetic resonance (NMR) (Li et al 2015), micro CT (Tiwari et al 2013) and ultra/small angle neutron scattering (USANS/SANS) (Yang et al 2017) to determine pore size distribution without any destructive contact with shale samples.

To make a better understanding of pore characteristics of shale from Sichuan Basin, in this paper, a range of multi scale approaches including CO_2 adsorption, N_2 adsorption and field emission scanning electron microscopy (FE-SEM) are used to analyse the Wufeng formation and Longmaxi Formation shale.

2 Geological Setting and Methodology

All the samples were collected from the Wufeng Formation and Longmaxi Formation in Ordovician and Silurian, which are marine resources in Sichuan Basin in southern China. At the moment of writing this paper, Weiyuan, Changning and Jiaoshiba shale gas pilots have already been activated in Sichuan Basin. The newer samples were drilled without water and were stored with dry preservation.

2.1 FE-SEM

To observe the pore structure, minerals and micro cracks, samples from both pilots were analysed with the use of FE-SEM. The device is a FEI Quanta 650 with energy dispersive X-ray spectroscopy (EDS). The accelerating voltage of the electron beam is set at 10KV and the detector is concentric higher energy electron detector (CBS). Before scanning them, the samples were cut by saws, polished, and then coated with carbon to increase their electrical conductivity.

2.2 Low pressure N_2 and CO_2 adsorption

Low pressure N_2 and CO_2 gas adsorption tests were launched on the Micromeritics 3 Flex. Samples were grounded and sieved to 1 - 3.5mm. Subsequently, they were deaerated at 300 degrees for 3 hours to remove the residual gas and free water. The equilibrium interval time selected was 30s for N_2 and 15s for CO_2, respectively. The relative pressure (p/p_0) was 0.005 - 0.995 for N_2 adsorption and 0.00006 - 0.013 for CO_2 adsorption. During the adsorption tests, the free spaces of the device were tested separately and the input was done manually. The N_2 and CO_2 adsorption isotherms were automatically measured by the device. The surface area, pore volume, and PSDs were then calculated based on various adsorption theories.

Brunauer et al (1938) proposed the BET method which is the most widely used for representing the surface area of porous media and powders:

$$\frac{1}{Q\left(\frac{p_0}{p}-1\right)}=\left(\frac{1}{v_m C}+\frac{C-1}{v_m C}\right)\frac{p}{p_0} \quad (1)$$

where Q is the specific adsorption quantity at relative pressure p/p_0, v_m is the monolayer adsorption capacity. C is a parameter about the adsorption heat. Generally, the BET equation is valid for low pressure N_2 adsorption within the p/p_0 of 0.05 - 0.3.

Lippens and de Boer (1965) proposed the t-plot method, which qualifies the determination of micro-pore volume, specific surface area and average pore size. It takes a reference t-plot from a number of non-porous with a C parameter similar to BET. Harkins and Jura statistical thickness equations are applied for the t plot method within a relative pressure of p/p_0 0.05 - 0.15. Through the graphical analysis of adsorption quantity versus average thickness of the statistical thickness of adsorption film t, we can obtain the t-plot.

The BJH method (Barrett et al 1951) takes the modified Kelvin method to calculate the pore size distribution of meso–pores and macro–pores. This method is based on the assumption that the pores are rigid, no micro pores exist and when the relative pressure is equal to 1, all pores are filled and suffused.

3 Results and Discussion

3.1 FE-SEM analysis

Generally, three kinds of pores can be found in shale reservoirs, including organic pores, intra-particle, and inter-particle pores, respectively (Loucks et al 2012). Figure 1a, b, c and d are taken from the WF shale sample, while 1d & e are taken from LMX sample. Figure 1b represents a partial enlarged view of Figure1a. FE-SEM images show that the organic matter (OM) and quartz are abundant in both WF and LMX formations. The widespread presence of quartz in shale gives a reasonable brittleness, making the shale fragile enough to be easily broken under hydraulic fracture.

Pyrite framboids with organic matter and intra-particle pores are widely distributed as illustrated in Figure 1a and d. Grid quartz mineral is commonly distributed around the organic matter and due to the squeezing and stretching during diagenesis, micro fractures appear at the boundary of quartz (Figure 1b and c). Pores in organic matter are significant for adsorbed gas and dissolved gas, and seem to be well developed (Figure 1d) with various geometric shapes such as cleat, honeycomb, cavernous, and irregular sphere. Organic pores are produced during the burial and maturation of diagenetic process. Organic matter exhibited in Figure 1f is formed with sliced clay minerals, suggesting that shale LMX formation suffered squeezing and that the OM migrated simultaneously with the mineral.

In Figure 1a, c, d and e, we can find a mass of inter-particle pores between rigid minerals with polygonal and elongated shapes. Inter-particle pores produced by flocculation, as a kind of original pores, are not evenly distributed in the shale formation. Dissolution of dolomite can also occur in shale formation and formed inter-particle pores (Figure 1e). Within a range hundreds of nanometers to microns, inter-particles can improve the connectivity (Figure 1a and e) and become an empty space to be filled with free gas.

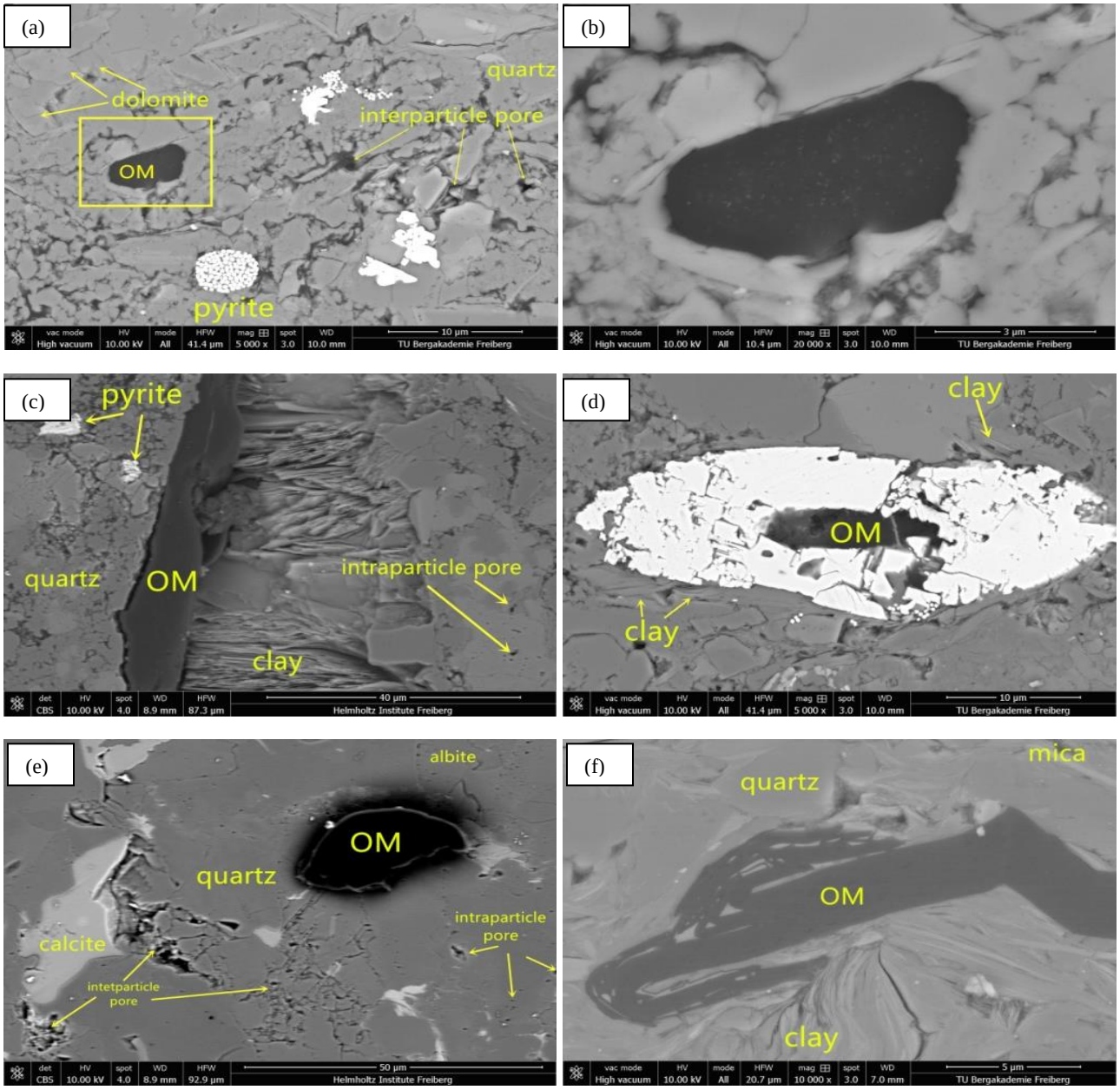

Figure 1 FE-SEM images for LMX and WF formation

In Figure 1c and e, we can observe irregular pores in mineral particles. Dissolution of dolomite and cleavage in mica consist the main sediment genesis of the intra-particle pores for LMX and WF formations. As a chemically unstable mineral, smectite generates a vast number of intra-particle pores during its transformation to an illite/smectite formation. Meanwhile, in Figure 1b, e and f, there are almost no pores in the organic matter. This may be due to the limited resolution of the FE-SEM or maybe the kerogen is immature.

3.2 Low pressure N_2 and CO_2 adsorption

Nitrogen isotherms for adsorption and desorption at 77K for the LMX and WF shale samples are presented in Figures 2 and 3, respectively. The highest quantity adsorbed at a relative pressure close to 1 is 6.66 cm^3/gr for the LMX shale and 10.81 cm^3/gr for the WF shale respectively. The adsorbed capacity always shows positive correlation with TOC (Cancino et al 2017).

At a low relative pressure, adsorption capacity demonstrates a gradual increase (type I isotherms from IUPAC) and reveals micro pores in shale samples. At a higher relative pressure, the isotherms belong to type Ⅱ isotherms from IUPAC classification. The shale sample as shown in FE-SEM images contain micro fracture and macro pores, and thus the horizontal plateau at relative pressure close to 1 is not present.

Obviously, both isotherms show adsorption hysteresis, meaning, the shale samples desorbed less gas than the adsorption process at the same pressure. This implies that both samples contain meso-pores. Theoretically, the desorption isotherm should always be above the adsorption

isotherm. It can be noted that the data regarding the adsorption isotherm for the LMX sample and a given relative pressure of 0.86 - 1 are not sufficient to show such a pattern. Both desorption branches demonstrate a lower closure point at any given relative pressure of or above 0.42. This can be described as a 'Tensile Strength Effect (TSE)' and is a consequence of stability limitation of the hemispherical meniscus during desorption in pores with critical diameters (approximately 4 nm) (Groen et al 2003). This effect of TSE always leads to artificial discrepancy for PSD calculated from nitrogen desorption branch using the BJH method at 4nm. According to the classification of IUPAC for adsorption hysteresis, both isotherms show H4 hysteresis, which is often associated with narrow slit pores (Sing and Williams 2004).

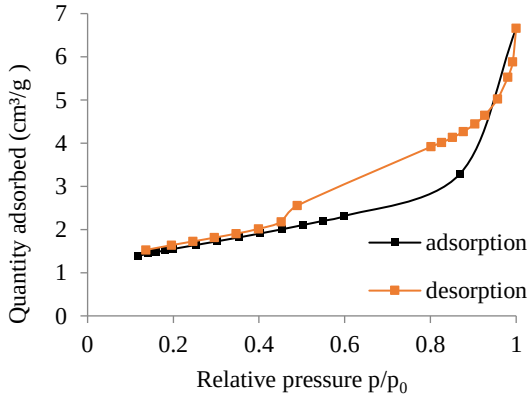

Figure 2 Adsorption-desorption isotherm of LMX shale

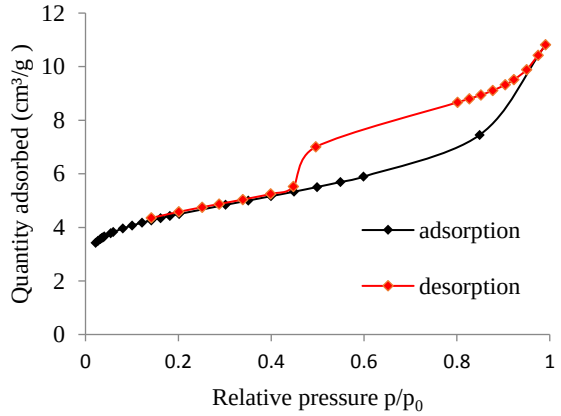

Figure 3 Adsorption-desorption isotherm of WF shale

The quadrupole moment of nitrogen molecules leads to interaction with adsorbent surface functional groups. This characteristic not only affects the orientation of adsorbed nitrogen molecules, but also influences the pressure for filling of micro-pores. For instance, initial stage of equilibrium relative pressure should be set as low as 10^{-7}. Under the ultimate low pressure, it is difficult to reach equilibrium with an extremely slow diffusion of nitrogen molecules in pores with a short time. Even worse, the pre adsorption of nitrogen can block the narrow throat. Resultantly, the filling pressure cannot quantificationally reflect the pore size of micro-pores.

Carbon dioxide with a kinetic diameter of 0.33nm can access smaller pores with rapid diffusion. Furthermore, the saturated vapor pressure of carbon dioxide is 3.5 MPa, meaning that we can get high resolution of micro-pores information during the medium pressure. The carbon dioxide isotherms for adsorption at 273K for the LMX and WF shale samples are depicted in Figure 4.

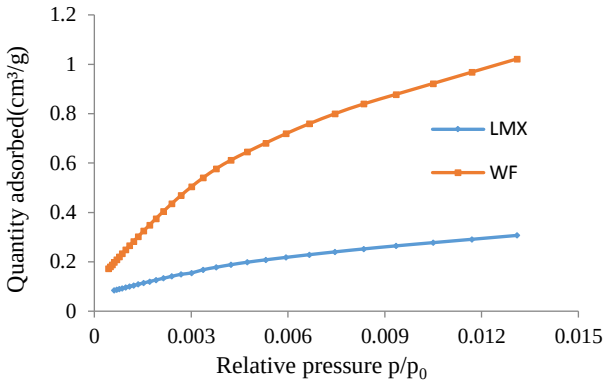

Figure 4 Carbon dioxide isotherms for adsorption at 273K

3.3 Specific surface area analysis

Specific surface areas from nitrogen and carbon dioxide isotherms are listed in Table 1. It should be noted at this point that nitrogen can access pores larger than 0.614nm, while the range of measurement of carbon dioxide is limited from 0.305 to1.475nm, at least theoretically.

Therefore, the S_{BET} value obtained from the BET method determines the total surface area of pores the diameter of which is larger than 0.614nm, while the S_{BJH} provides the information for pores within a range of 1.7-300nm. The S_{mic} derived from t-plot by nitrogen isotherms shows the specific surface area of micro pores ranging from 0.6nm to 2nm. Additionally, the S_{ext} value shows the specific surface area of pores with diameter larger than 2nm. Meanwhile, S_{co2} from isotherms of carbon dioxide reveals the specific surface area for micro pores from about 0.3 to 1.5 nm in diameter. The S_{co2} is calculated via the D-A method and is slightly higher than the S_{mic} value derived from the t-plot method, which in turn indicates that the micro pores (especially within a diameter of 0.3-1.5nm) in both shale samples are abundant.

The total specific surface areas calculated via the BET method (S_{BET}) for the LMX and WF shale samples are 5.47 m^2/gr and 16.33cm^2/gr, respectively. The S_{BJH} surface areas derived from the application of the BJH method (4.69m^2/gr, 8.72 m^2/gr, respectively) are slightly lower than the BET figures. This is due to the fact that the probed pore range (0.614 nm to 300 nm) in the BET method is greater than the analysis range (1.7 nm to 300 nm) of the BJH method. We can roughly estimate the specific surface area (given a pore size diameter from 0.6nm to 1.7nm) for the LMX and WF formations at 0.78m^2/g and 7.61m^2/gr, respectively, based

on the assumption that the macro-pores make negligible contribution to the total surface area.

Table 1 Specific surface area from different method

Method	BET	t-plot		BJH	D-R
S(m^2/gr)	S_{BET}	S_{mic}	S_{ext}	S_{BJH}	S_{co2}
Range (nm)	0.6-300	0.6-2	2-300	1.7-300	0.3-1.5
LMX	5.47	1.26	4.21	4.69	3.29
WF	16.33	7.78	9.54	8.72	11.97

3.4 Pore volume and pore size distribution analysis

The pore volumes calculated with the t-plot method (micro pores range 0.6-2nm), BJH method (meso-macro pores range 2-300nm) and D-A method (micro pores from carbon dioxide range 0.3-1.5nm) are illustrated in Table 2.

In the LMX formation, the adsorption capacities of nitrogen and carbon dioxide are quite lower than in the WF formation. The indications for the specific surface area and pore volume show clearly that the pores in the LMX formation are not so abundant as in the WF formation. The meso−pores and macro−pores are the major contributors to the pore volumes for the samples in both formations.

Table 2 Pore volume of LMX and WF formation

Method	T-plot V_{mic}/cm^3	BJH $V_{mes-mac}/cm^3$	D-A V_{mic}/cm^3
Range (nm)	0.6-2	2-300	0.3-1.5
LMX	5.81	6.932	4.014
WF	2.833	10.766	6.068

The pore size distribution for both samples regarding N_2 and CO_2 are illustrated in Figures 5 - 8. Being an immature gas shale, the LMX formation holds less micro−pores than the WF formation, as shown in the qualitative analysis conducted using the FE-SEM. The distribution of micro−pores is merely about 1nm in diameter for both formations' samples. For meso−pores, the WF formation has a range smaller than 20nm, while meso−pores in the LMX formation range from 2nm to 30nm. The LMX formation holds a wide range of pore sizes, but with less pores volume and surface area than in the WF formation.

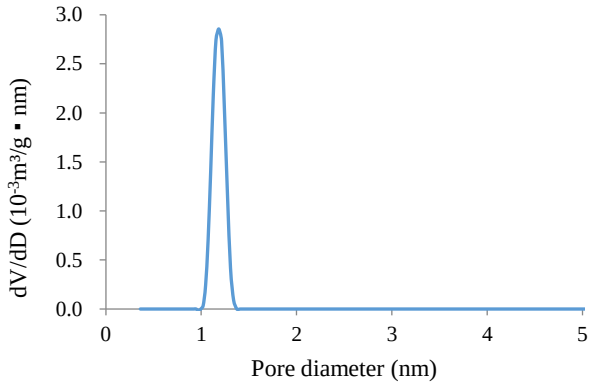

Figure 5 Pore size distribution of CO_2 for LMX sample

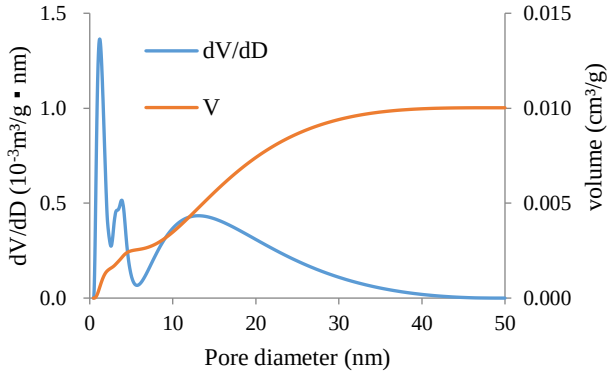

Figure 6 Pore size distribution of N_2 for LMX sample

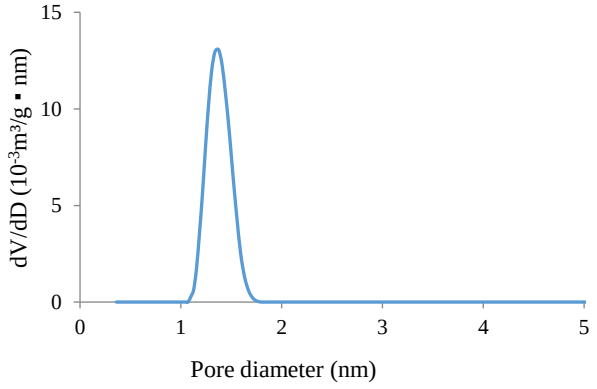

Figure 7 Pore size distribution of CO_2 for WF sample

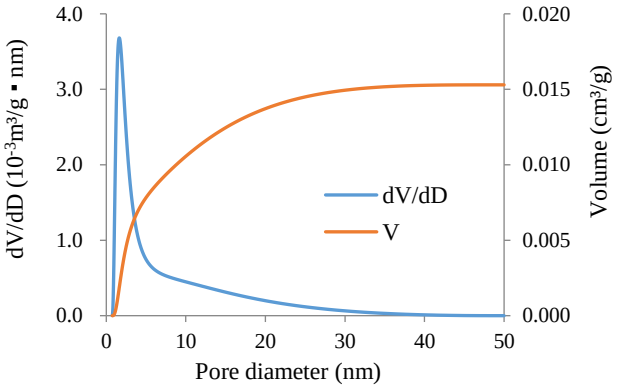

Figure 8 Pore size distribution of N_2 for LMX sample

4 Conclusions

FE-SEM and low pressure nitrogen and carbon dioxide adsorption were applied to reveal pore characteristics of Longmaxi and Wufeng shale formations. FE-SEM images show that both samples contain inorganic pores, though organic pores in LMX samples are absent. Low pressure nitrogen and carbon dioxide analysis showed that the pore size distribution for the LMX formation ranges from 1nm to 30nm. For the WF formation, the pore size distribution varies between1nm - 20nm and most pores are smaller than 10nm. Micro-pores are a major contributor to the specific surface area, while the meso-and macro-pores compose volumes for both samples.

Acknowledgement

The authors gratefully acknowledge the financial support from China Scholarship Council.

Reference

Ambrose R.J., R.C. Hartman, M. Diaz-Campos, I.Y. Akkutlu and C.H. Sondergeld, 2012. Shale gas-in-place calculations Part I: New pore-scale considerations. SPE Journal, **17**(**1**): 219 - 229.

Brunauer S., P.H. Emmett and E. Teller, 1938. Adsorption of gases in multimolecular layers. Journal of the American Chemical Society, **60**(**2**): 309 - 319.

Bernard S., L. Brown, R. Wirth and A. Schreiber, 2013. 7 FIB-SEM and TEM investigations of an organic-rich shale maturation series from the lower toarcian posidonia shale, Germany: Nanoscale Pore System and Fluid-rock Interactions. AAPG. **102**: 53 - 66.

Barrett E. P., L.G. Joyner and P.P. Halenda, 1951. The determination of pore volume and area distributions in porous substances. I. Computations from Nitrogen Isotherms. Journal of the American Chemical Society, **73**(**1**): 373 - 380.

Cancino O. P. O., D. P. Mancilla, M. Pozo, E. PErez and D. Bessieres, 2017. Effect of organic matter and thermal maturity on methane adsorption capacity on shales from the Middle Magdalena Valley Basin in Colombia. Energy & Fuels, **31** (**11**): 11698 - 11709.

Groen J.C., L.A.A. Peffer and J. Pérez-RamíRez, 2003. Pore size determination in modified micro- and mesoporous materials. Pitfalls and limitations in gas adsorption data analysis. Microporous & Mesoporous Materials, **60**(**1**): 1 - 17.

Houben M.E.**,** A. Barnhoorn, L. Wasch, J. Trabucho-Alexandre, C.J. Peach and M.R. Drury, 2016. Microstructures of early Jurassic (Toarcian) shales of Northern Europe. International Journal of Coal Geology, **165**: 76 - 89.

Javadpour, F., M. M. Farshi and M. Amrein, 2012. Atomic-force microscopy: A new tool for gas-shale characterization. Journal of Canadian Petroleum Technology, **51**(**04**): 236 - 243.

Kelly S., H. El-Sobky, C. Torres-Verdín and M.T. Balhoff, 2016. Assessing the utility of FIB-SEM images for shale digital rock physics. Advances in Water Resources, **95**: 302 - 316.

Li J., J. Yin, Y. Zhang, S. Lu, W. Wang, J. Li, F. Chen and Y. Meng, 2015. A comparison of experimental methods for describing shale pore features - A case study in the Bohai Bay Basin of eastern China. International Journal of Coal Geology, **152**: 39 - 49.

Lippens B. C. and J. H. de Boer, 1965. Studies on pore systems in catalysts: V. The *t* method. Journal of Catalysis, **4**(**3**): 319 - 323.

Loucks R.G., R.M. Reed and S.C. Ruppel, 2012. Spectrum of pore types and networks in mud rocks and a descriptive classification for matrix-related mud rock pores. AAPG Bulletin, **96**(**6**): 1071 - 1098.

Sing K.S.W. and R.T. Williams, 2004. Physisorption hysteresis loops and the characterization of nanoporous materials. Adsorption Science and Technology, **22**: 773 - 781.

Wu, T., X. Li, J. Zhao and D. Zhang, 2017. Multiscale pore structure and its effect on gas transport in organic-rich shale. Water Resources Research., **53**(**7**):5438 - 5450.

Yang R., S. He, Q. Hu and J. Yi, 2017. Applying SANS technique to characterize nano-scale pore structure of Longmaxi shale, Sichuan Basin (China). Fuel, **197**: 91 - 99.

Zou C., D. Dong, S. Wang, J. Li, X. Li, Y. Wang, D. Li and K. Cheng, 2010. Geological characteristics, formation mechanism and resource potential of shale gas in China. Petroleum Exploration and Development, **37**(**6**): 641 - 653.